Proceedings of the Design Society, Volume 6: DESIGN 2026
https://doi.org/10.1017/pds.2026.10561

Design guidelines for electrical conductors and Joule-heating structures fabricated additively by material extrusion

Maximilian Nowka[1,✉], Marvin Bergner[1], Till Hecker[1], Katja Ruge[1], Karl Hilbig[1], Wei-Song Hung[2] and Thomas Vietor[1]

[1] Institute for Engineering Design, Technische Universität Braunschweig, Germany, [2] Graduate Institute of Applied Science and Technology, National Taiwan University of Science and Technology, Taiwan

✉ m.nowka@tu-braunschweig.de

ABSTRACT: Additive Manufacturing (AM) enables the local adjustment of material properties using multi-material strategies, especially with Material Extrusion (MEX). Electrically conductive structures like conductors, Joule heating structures, and their transitions can be realised with conductive polymer composites (CPC). However, specific Design for Additive Manufacturing (DfAM) guidelines for the afore mentioned structures are still missing. This work uses experimental data by thermography and the measurement of resistivity to derive twelve design rules. The rules are applied to an application example.

KEYWORDS: design guidelines, additive manufacturing, joule-heating, material extrusion, electrically conductive polymer composite

1. Introduction

Additive Manufacturing (AM) offers significant design freedom for products with functional integration, complex geometries and hierarchical structures (Gibson et al., 2021; Rosen, 2007). Among these technologies listed in DIN EN ISO/ASTM 52910:2020-02, Material Extrusion (MEX-TRB/P) of polymers is particularly relevant due to its selective material deposition enabling complex multi-material structures. This capability is increasingly used to realise electrical functions with conductive polymer composites (CPC), including current-carrying leads and Joule-heating elements.

Most work emphasises materials and processing (Masarra et al., 2022; Nowka et al., 2024; Paz et al., 2020; Stankevich et al., 2023; Truman et al., 2020; Watschke et al., 2019) while a few studies explore the impact of the design of the electrical structures on the resulting product performance (Barši Palmić et al., 2020; Kim et al., 2017; Kwok et al., 2017; Nassar & Dahiya, 2021; Tan & Low, 2018). A systematic investigation of basic design principles has not been conducted.

Fundamental Design for Additive Manufacturing (DfAM) guidelines are therefore missing for three interdependent structure types: low-loss conductors, heating elements with spatially controlled, homogeneous heat generation and transitions that suppress localised hotspots. This work addresses this gap by experimentally investigating 2D and 2.5D geometric factors and by linking path planning to current-density homogeneity. Based on resistivity measurements and thermographic analysis, practical design rules are derived, supporting higher conductivity, reduced hotspots, and more robust products and forming a basis for standardised DfAM of electrically functional MEX structures.

2. Acquisition of data for the design exploration approach

The following section presents the design of experiments, the set-up of the Additive Manufacturing process and the experimental design.

https://doi.org/10.1017/pds.2026.10561 Published online by Cambridge University Press

2.1. Materials, processing by additive manufacturing and specimen preparation

Table 1 provides an overview of the electrically conductive composites used, including their composition and the constant processing parameters used for the manufacturing of specimens.

Table 1. Overview of the composites and AM processing parameters

Composite name	Polymer	Conductive filler	Extrusion [°C]	Buildplate [°C]	Speed [mm/s]
Multi3d Electrifi	PCL	CuP	140	RT	20
Koltron G1	PVDF	G	287	60	15
Conductive Filaflex	TPU	CB	250	55	20
Ampere PLA	PLA	CNT, CB, Gr	235	50	25
Alfaohm	PLA	CNT, CB, Gr	215	60	30
Protopasta Conductive PLA	PLA	CB	210	60	35
3dkonductive electroconductive	PLA	CB	215	65	40
FILI conductor	PLA/TPU	Gr	260	RT	40
Eel 3D Printing Filament	TPU	CB	230	32	15

Polymers: PCL = polycaprolactone; PLA = polylactic acid; PVDF = polyvinylidene fluoride, TPU = thermoplastic polyurethane. Conductive fillers: CuP = copper particles; G = graphene; CNT = carbon nanotubes; CB = carbon black; Gr = graphite. RT = room temperature (23 ± 1°C).

Before additive processing, all filaments were dried for 48 hours. The specimens were fabricated using a toolchanger system equipped with Hemera direct drive filament extruders and hardened, coated 400 µm nozzle X (E3D-Online, Chalgrove, Oxfordshire, United Kingdom). The G-code was generated using SuperSlicer 2.4 (based on PrusaSlicer, Prusa Research, Prague, Czech Republic). Following the recommendations of Nowka et al. (2025) for CPCs the layer height (200 µm) equaled 50% of the 400 µm nozzle diameter. The thickness of the specimens was measured and only those within the ± 5% tolerance range defined by DIN EN ISO 3915:2022-5 are included in the analysis.
To minimise the contact resistance colloidal silver ink EMS#12640 (Electron Microscopy Sciences, Hatfield, PA, USA) was used as an electrical bonding agent. For Koltron G1, to which the ink does not adhere, conductive epoxy 8331D-14G (MG Chemicals Ltd., Burlington, ON, Canada) was used.

2.2. Test rig for the resistance measurement and thermography

Depending on the objective, the specimens are analysed for either their resistivity or heat distribution within electrically conductive structures. The test rig (Nowka, Ruge, et al., 2024) is shown in Figure 1:

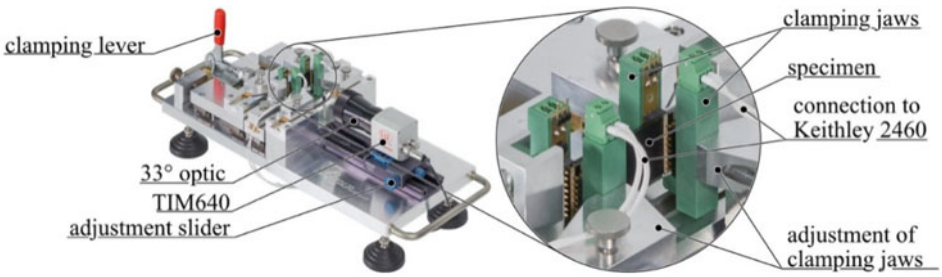


Figure 1. Test rig for electrical resistance measurements and thermographic imaging

The test rig utilises spring-loaded contacts, ensuring repeatable testing conditions such as consistent contact force between the specimen and the source meter. Electrical resistance is measured according to DIN EN ISO 3915:2022-5 using a four-wire measurement technique with a Keithley 2460 Sourcemeter (Keithley Instruments, Solon, OH, USA) at 23 ± 1°C and a measurement current of 100 µA. The resistivity ρ is calculated from the measured resistance R, the conductive cross-sectional area A and the length L between the inner contact surfaces using the following Equation (1):

https://doi.org/10.1017/pds.2026.10561 Published online by Cambridge University Press

$$\rho = R \cdot \frac{A}{L} = \frac{1}{\sigma} \tag{1}$$

The reciprocal of resistivity ρ is called conductivity σ. The evaluation of current density homogeneity is conducted qualitatively using thermographic imaging. Areas with higher current density are expected to exhibit elevated temperatures. To ensure comparability, the specimens are heated with a constant power and once the rated power is reached within ± 2%, a thermogram is taken automatically with a defined delay. Thermal images are recorded using a TIM 640 thermal imaging camera (640 × 480 px) with 33° optics (Micro-Epsilon Messtechnik GmbH & Co. KG, Ortenburg, Germany) at object distances of 100 mm and 125 mm, yielding resolutions of approximately 62 µm/px and 77.5 µm/px, respectively.

2.3. Influence of number of strands on resistivity

The width of electrically conductive structures affects their cross-sectional area, making it a critical design parameter. Two studies suggest that the number of parallel strands can significantly influence the resistivity of structures made by MEX (Truman et al., 2020; Zhang et al., 2017). Therefore, an extensive study with nine composites and finer strand-number gradations was conducted. Rectangular (60 × 24 mm), single-layer (200 µm) specimens with 0° infill to the measurement direction were fabricated. Figure 2 shows representative specimens and the schematic measurement setup.

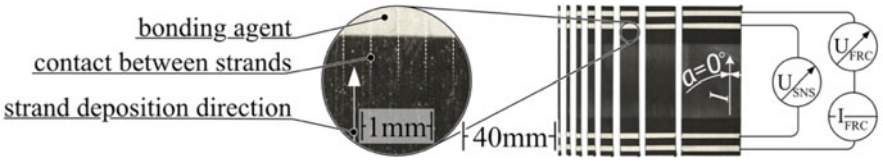


Figure 2. Alfaohm specimens with 1 to 67 strands (from left to right)

The number of parallel strands was varied, producing specimens with 1, 2, 3, 5, 8, 13, 21, 34, and 67 strands. For each parameter set, seven specimens were fabricated. The results are presented in Figure 3:

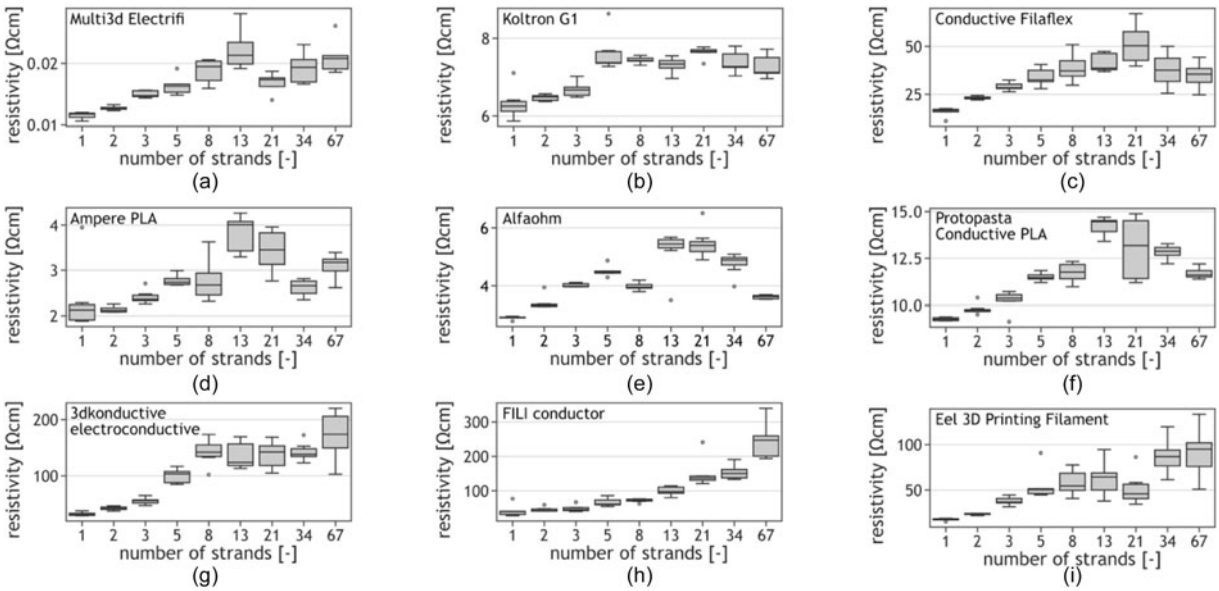


Figure 3. Influence of number of strands on resistivity across composites: (a) Multi3d Electrifi; (b) Koltron G1; (c) Conductive Filaflex; (d) Ampere PLA; (e) Alfaohm; (f) Protopasta Conductive PLA; (g) 3dkonductive electroconductive; (h) FILI conductor; (i) Eel 3D Printing Filament

All composites show the lowest resistivity for single-strand conductors. With increasing strand count, resistivity first rises, then either reaches a plateau (Figure 3a–g) or continues to increase (Figure 3h-i), indicating that the chosen parameter range may be too narrow for some materials. In all cases, variability grows with strand number. Alfaohm, combining high conductivity with low variance, was used in subsequent experiments.

https://doi.org/10.1017/pds.2026.10561 Published online by Cambridge University Press

2.4. Influence of conductor design on current-density homogeneity

The primary function of electrical conductors is to transmit current between two points with minimal losses. This experimental series aims to determine the influence of 2D and 2.5D geometric factors on the homogeneity of current distribution within the conductor.

To approximate a path-planning strategy aligned with the current flow, all strands are deposited parallel to the neutral axis (Figure 4), thereby avoiding adverse effects of inter-strand contact resistance. Extrusion process parameters (Table 1) are kept constant. The specimens are 5 mm wide, 200 µm thick, manufactured as single-layer structures made from Alfaohm, and both contact areas are coated with silver ink to minimise contact resistance between the specimen and the measurement setup.

The varied design parameter in this study is the conductor geometry. Discontinuous layouts and continuous layouts based on Bézier splines are investigated. For discontinuous conductors, the varied design factors are the deflection angle θ (30°–120° in 15° increments) from the straight path and the corner modification. Bisecting chamfers (lengths 1, 2, 5, 10 mm) and fillets (radii 1, 2, 5, 10 mm) are examined. For Bézier splines, the aspect ratio A (1, 2, 3) and the relative control point position d_{cp} (25%–100% in 25% increments) are varied, with tangential continuity enforced at the start and end points. The design concepts and measurement setup are shown in Figure 4.

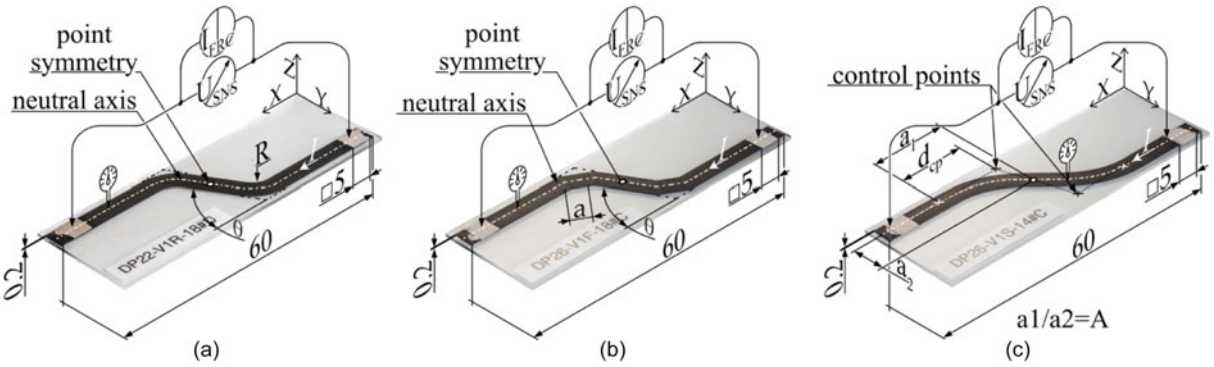


Figure 4. Design concepts for AM conductor path planning: (a) discrete with radius; (b) discrete with chamfer; (c) continuous Bézier spline

Geometry and dimensions influence the current distribution and, consequently, the heat generation within the conductors. The evaluation is based on thermographic imaging. Thermographic images are recorded at a power input of 1500 mW with a trigger delay of 1 s. The short duration between the onset of heating and image acquisition ensures that the results are only marginally affected by heat conduction from local hotspots to cooler regions. The following figures present the thermograms obtained from the three experimental series.

Figure 5 shows thermograms of discontinuous conductors with radii as corner modifications.

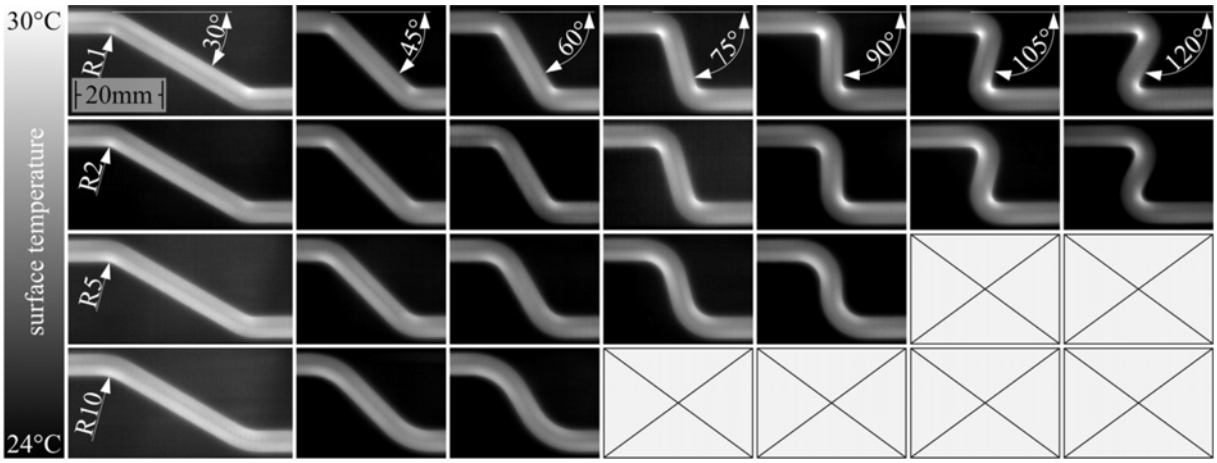


Figure 5. Thermographic images of specimens with discontinuous paths (see Figure 4a), for varying angles θ and radii R. Recorded at 1500 mW after 1 s. ☒ = geometrical not realisable

https://doi.org/10.1017/pds.2026.10561 Published online by Cambridge University Press

The thermographic images in Figure 5 reveal two key trends. First, sharper deflection angles generate more pronounced hotspots on the inner edge of the conductor, accompanied by corresponding cold spots on the outer edge. These cold spots, located opposite the hotspots, exhibit significantly lower temperatures and thus indicate a reduced contribution to current transport. Second, increasing the corner radius decreases hotspot intensity and distributes the elevated temperature over a larger area, indicating a reduction in local current density.
Figure 6 shows thermograms of discontinuous conductors with chamfers as corner modifications.

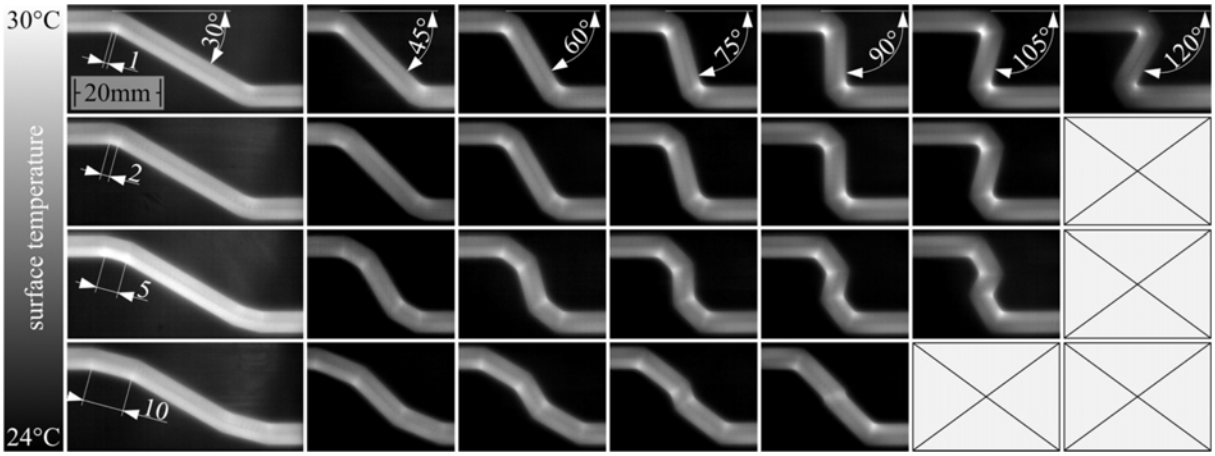


Figure 6. Thermographic images of specimens with discontinuous paths (see Figure 4b), for varying angles θ and chamfer lengths a. Recorded with 1500 mW after 1 s. ☒ = geometrical not realisable

As with the radii, two trends are evident. First, larger deflection angles θ lead to more pronounced hotspots. Chamfers generally reduce hotspot intensity by smoothing sharp transitions. However, their effect is notably weaker than that of radii. Even for large chamfer lengths, distinct hotspots remain. Compared to hotspots formed by radii (cf. Figure 5), hotspots occurring in chamfered regions appear sharper and extend over a larger portion of the track width.

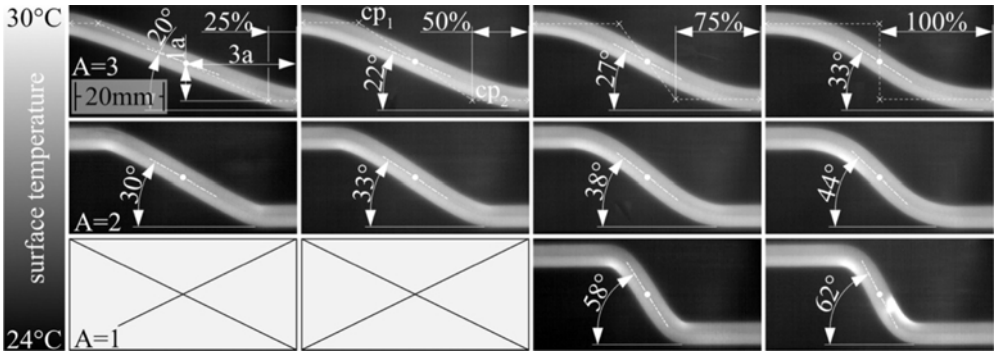


Figure 7. Thermographic images of specimens with continoues Bézier splines shown in Figure 4c, with varying aspect ratios A (=a_1/a_2) and control point (cp) distances. Recorded with 1500 mW after 1 s. The tangent slope angles serve as reference for comparison. ☒ = geometrical not realisable

Figure 7 shows the thermographic images of continuous conductors following Bézier spline paths.
At first glance, spline-based conductors appear more homogeneous than the previously discussed layouts. However, a visual comparison of the tangent slopes between the two turning points reveals that the hotspot characteristics are similar to those of discontinuous paths with comparable local gradients. This is particularly evident for spline variants with an aspect ratio A = 1 and control point distances of 75% and 100%, which closely resemble the behaviour of the 60°/R2 radius configuration (cf. Figure 5). Splines therefore do not inherently outperform or underperform comparable discontinuous geometries with radii. Instead, their main advantage lies in robustness and usability: spline paths between defined start and end points are generated automatically according to boundary conditions, making them less sensitive to dimensional changes and reducing the need for expert tuning of geometric parameters.

https://doi.org/10.1017/pds.2026.10561 Published online by Cambridge University Press

2.5. Design of heat generating structures

Heating structures are intended to convert electrical energy into (homogeneously distributed) thermal energy within a targeted area. The objective of this experimental series is to investigate various design approaches for spatially localised and homogeneous heat generation. The thermal power P generated by an additively manufactured heating structure can be influenced by a combination of design and manufacturing parameters, as expressed in Equation (2):

$$P = \frac{(\Delta U)^2}{\rho(\rho_F, B_{1\ldots n}, P_{1\ldots n}) \cdot \frac{L}{A}} \tag{2}$$

Here, the voltage drop ΔU across the heating structure is determined by the external system voltage and the resistances of other components in the circuit. The overall resistivity ρ of the structure depends significantly on the feedstock resistivity ρ_F (Nowka et al., 2023), the path planning parameters $B_{1\ldots n}$ (Nowka et al., 2025) and the extrusion parameters $P_{1\ldots n}$ (Nowka et al., 2024) used during the additive manufacturing process. While the influence of these AM parameters on the resulting resistivity has been extensively studied (Barši Palmić et al., 2020; Paz et al., 2020; Stankevich et al., 2023; Watschke et al., 2019), this work focuses on the geometric factors, specifically the effective conductor length L and the cross-sectional area A, which directly impact the overall electrical resistance. Figure 8 groups the concepts into several categories and illustrates specific implementation variants for each.

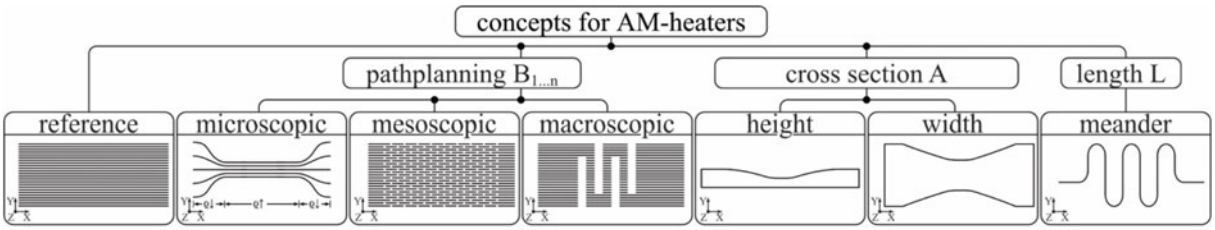


Figure 8. Design concepts for heating structures in additive manufacturing

The group of path-planning concepts comprises several approaches to increase resistivity by controlling material placement. On the microscopic scale, resistivity can be increased by arranging strands in close proximity and thereby raising the overall resistance, as discussed in Section 2.3. On the mesoscopic scale, intentionally interrupting individual strands forces the current through inter-strand contact interfaces, increasing contact resistance and thus heat generation within and between layers. On the macroscopic scale, the current path is further manipulated by separating larger strand bundles, forcing current through orthogonal infill patterns, which exhibit higher resistivity than parallel arrangements (Hohimer et al., 2020).

Local resistance can also be increased by reducing the electrically conductive cross-sectional area A, either by decreasing strand height or width in the heating region. A further option is to extend the effective conductor length L using meander-like paths, which enforce a longer, more resistive current trajectory.

Due to differences in volume and surface area, the thermograms of the heating structures are not directly comparable in a quantitative manner. To enhance qualitative comparison, all specimens are driven at 750 mW, and thermograms are recorded after 30 s, ensuring that the temperature distribution has reached steady state. The resulting temperature distributions are shown in Figure 9.

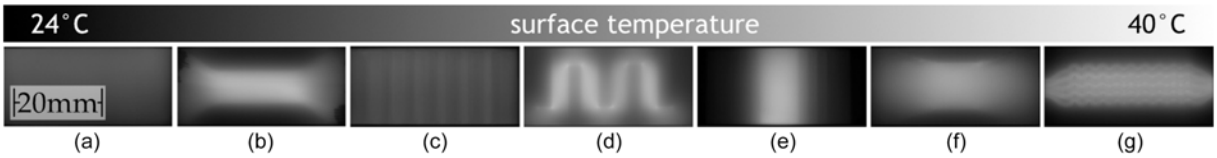


Figure 9. Infrared thermograms of various heating structures: (a) reference; (b) microscopic; (c) mesoscopic; (d) macroscopic; (e) height variation; (f) width variation; (g) meander

https://doi.org/10.1017/pds.2026.10561 Published online by Cambridge University Press

The microscopic heating structure (Figure 9b) relies on locally concentrated strand arrangements to tailor resistivity and exhibits well-defined, localised, and homogeneous heating. The mesoscopic structure (Figure 9c) is geometrically similar to the plate-like reference heater (Figure 9a) yet exhibits slightly less homogeneous heating due to contact resistance at internal transitions. The design with macroscopic slots (Figure 9d) shows pronounced hotspots at the slot edges. The upper and lower regions conduct along the strand direction, while the central region forces current perpendicular to the strands through higher inter-strand contact resistance, resulting in targeted heating but hotspot prone transitions. The vertical taper (Figure 9e) enables the most precise heat localisation, as the discrete reduction in cross-section in 200 µm steps along the build direction (staircase effect) produces well-defined heating zones. In contrast, the horizontal taper (Figure 9f) yields more diffuse edge heating due to the continuous cross-sectional change in the xy-plane. Several specimens (Figures 9a and c) distribute the applied power over a larger area and therefore appear cooler.

2.6. Design of transition structures between different geometries

Heating structures are often large-area by design to achieve good heat transfer, whereas conductors are kept compact to conserve space. This necessitates transition structures that enable a continuous change in both geometry and electrical resistance between conductor and heater, thereby avoiding hotspots in the transition region. An ideal transition exhibits high spatial selectivity: the conductor region remains cold, while the temperature at the beginning of the heating structure matches that of the remaining heater. Various concepts for such transition structures are shown in Figure 10.

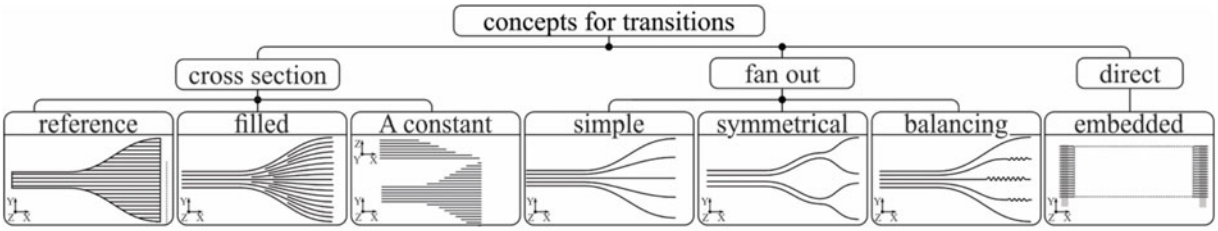


Figure 10. Design concepts for continuous transition structures between electrically conductive elements of dissimilar geometry

The simplest approach to increase the transition area is a straightforward widening of the conductor to the full width of the heating structure while maintaining the 0° infill orientation of the conductor. An improved variant, the so-called filled concept, distributes the conductive strands equidistantly and fills the remaining gaps with parallel strands to promote a more uniform current distribution. Another concept keeps the total cross-sectional area constant by varying strand width and height. Fan-out concepts deliberately split and spread individual strands to avoid local constrictions; in the symmetrical and balancing variants, all strands additionally share the same length. A special case is the direct transition from a conventional conductor to an additively manufactured heating structure.

Depending on the design, these concepts are suited for different heater types. Fan-out concepts are particularly suitable for meandering or highly branched layouts such as the microscopic, mesoscopic, and meander structures (cf. Figure 8), whereas cross-section and direct approaches are preferred for planar heaters such as the reference, macroscopic, or variable height and width structures. Figure 11 shows thermographic images of transitions from a conductor to a heating structure.

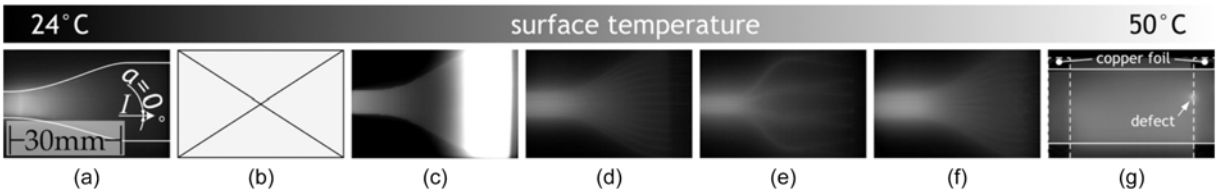


Figure 11. Thermographic images of transition structures: (a) transition without modifications (reference); (b) not investigated; (c) constant cross-section; (d) flared transition; (e) symmetric flaring; (f) flaring with length compensation; (g) direct contact

https://doi.org/10.1017/pds.2026.10561 Published online by Cambridge University Press

The transition structure in Figure 11a widens the conductor to the heater width at a constant 0° infill angle and serves as reference. The concept in Figure 11b is based on fanning out individual strands and filling the gaps but was not fabricated or evaluated due to its complex path planning. The heater in Figure 11c uses a geometric transition: the current supplying conductor is manufactured in multiple layers and becomes thinner as it widens toward the heater. Owing to the larger conductive cross-section, the losses and consequently the temperature in the conductor and transition region are significantly lower than in the heating zone. The concepts in Figures 11d to f fan out the strands equidistantly, with basic, symmetrical, and length-balanced layouts. This results in a more homogeneous current density in the heater. The design in Figure 11g is unique in that the heating structure is printed directly onto a conventional conductor, which simultaneously functions as the external electrical interface. Due to the high conductivity of the conventional lead, losses occur primarily at the interface, while the additively manufactured heater exhibits a highly uniform temperature and current-density distribution.

3. Derivation of design guidelines from the experimental data

Based on the experimental findings, design guidelines for AM can be derived. Table 2 summarises these guidelines in four categories: general recommendations, which apply universally, and specific guidelines for conductors, heating structures and transition structures.

Table 2. Design for Additive Manufacturing guidelines for electrically conductive structures derived from experimental data

No.	Category		Rule description
1	General		Use two or more contacting parallel strands to increase redundancy and failure tolerance.
2			Dimension conductive areas as integer multiples of the nozzle diameter to ensure uniform area fill.
3			To minimise resistivity, align individual strands parallel to the current flow.
4	Connections		Route conductors along spline paths to reduce resistive losses and simplify the design process.
5			For conductor geometries with corners, apply fillets to reduce hotspot intensity.
6			Increase corner radii with increasing conductor width to avoid hotspots.
7			To maximise conductivity, minimise the number of contacting parallel strands.
8			For discontinuous conductor layouts, use shallow deflection angles.
9	Heaters		Employ meander layouts to achieve homogeneous heating in heaters with complex outer geometries.
10			Use planar (area-filling) heater structures to maximise heat output.
11	Transitions		Apply balanced fan-out transition concepts for meandering heating structures.
12			Use cross-section-based transition concepts for planar heating structures.

https://doi.org/10.1017/pds.2026.10561 Published online by Cambridge University Press

Some design guidelines are inherently conflicting. For example, increasing reliability by using multiple parallel paths opposes minimising specific resistance by reducing the number of adjacent strands. Depending on the design objective, the relevance and weighting of individual guidelines must therefore be carefully balanced.

4. Application example

As a practical application, a non-heated mirror is modified with an additively manufactured backside heating structure. The goal is to integrate the heater without redesigning the mirror mount, ensuring the surface reaches at least 35°C to evaporate condensed water. To avoid additional insulation or touch protection, the system is designed for 10 W peak power at a voltage below 60 V ensuring electrical safety. A meander-shaped heater is selected to cover the irregular backside with a compact footprint while maintaining homogeneous heating. It is divided into two zones with equal electrical resistance and thus identical heating power. The meander amplitude is adapted to maintain constant resistance along each branch, avoiding hotspots. A fanned-out transition connects the main conductor to the heater. The electrical interface is realised with conductive epoxy. The demonstrator is shown in Figure 12.

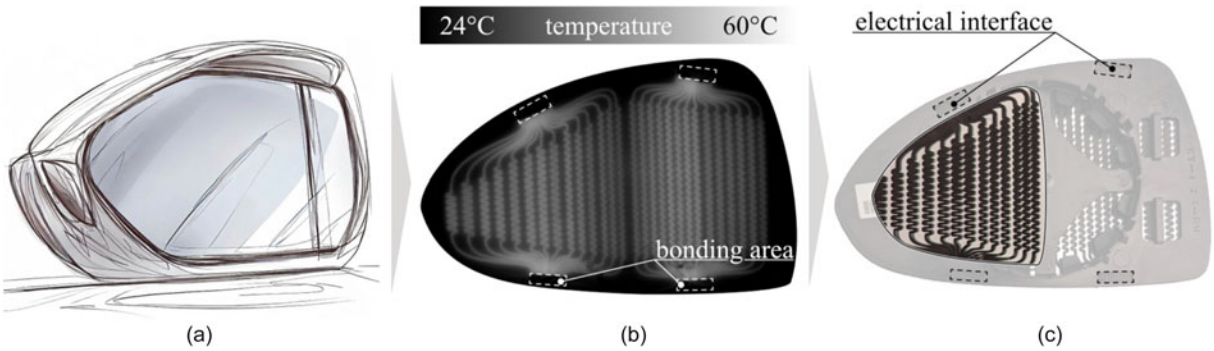


Figure 12. Demonstrator: (a) design concept; (b) validation of the Joule-heating structure by thermography; (c) integrated modified mirror in assembly

The convex backside of the mirror results in a non-planar surface for the MEX process. The surface is therefore probed, and the measured profile is used to adapt the nozzle distance during extrusion, ensuring uniform layer thickness and adhesion. Thermography (Figure 12b) confirms homogeneous heating, and Figure 12c shows the integrated system in the assembled state.

5. Conclusion

This study established foundational design guidelines for conductors, Joule-heating structures and as a novel design aspect their transitions fabricated using MEX. The key findings are derived from experimental resistivity measurements, thermographic analysis, and systematic design exploration:

- **Influence of strands side-by-side on resistivity**: The number of strands placed side by side influences the resistivity regardless of the composite used. Depending on the composite, this effect stabilises once a certain threshold number of strands is reached.
- **Conductors path optimisation**: Geometric smoothness, such as the use of splines or large radii, proved effectiveness in reducing localised hotspots and promoting uniform current distribution.
- **Heating structure design**: Heating elements require a balanced approach, where structure size and current path length significantly impact heat distribution. The results demonstrated that continuous, smoothly varying paths yield more homogeneous thermal profiles.
- **Transition structures**: Transitions between compact conductive paths and broader heating structures were achieved by introducing gradual width changes and optimised path planning, significantly reducing thermal stress concentrations (hotspots).

These insights provide a first step toward design rules for MEX-based conductive components, supporting the further integration of functional materials into additively manufactured systems.

https://doi.org/10.1017/pds.2026.10561 Published online by Cambridge University Press

Acknowledgement

This work is supported by the German Research Foundation (DFG) under grant numbers 452679573 and 452009430, and by the German Federal Ministry of Economics and Energy (BMWE) under grant number 16KN112736, and by a joint seed funding initiative by National Taiwan University of Science and Technology and TU Braunschweig. The funding sources had no influence on the study. We would like to thank Christopher Gassen for his help with the photography.

Data Availability

The data, models and figures presented in the study are openly available in FigShare at: https://doi.org/10.6084/m9.figshare.30620111

References

Additive Fertigung—Konstruktion—Anforderungen, Richtlinien und Empfehlungen (Nummer DIN EN ISO/ASTM 52910:2020-02). (2020). Beuth Verlag GmbH.

Barši Palmić, T., Slavič, J., & Boltežar, M. (2020). Process parameters for FFF 3D-printed conductors for applications in sensors. *Sensors*, 20(16), 4542. https://doi.org/10.3390/s20164542

Gibson, I., Rosen, D. W., Stucker, B., & Khorasani, M. (2021). *Additive Manufacturing Technologies*. Springer.

Hohimer, C. J., Petrossian, G., Ameli, A., Mo, C., & Pötschke, P. (2020). 3D printed conductive thermoplastic polyurethane/carbon nanotube composites for capacitive and piezoresistive sensing in soft pneumatic actuators. *Additive Manufacturing*, 34, 101281. https://doi.org/10.1016/j.addma.2020.101281

Kim, K., Park, J., Suh, J., Kim, M., Jeong, Y., & Park, I. (2017). 3D printing of multiaxial force sensors using carbon nanotube (CNT)/thermoplastic polyurethane (TPU) filaments. *Sensors and Actuators A: Physical*, 263, 493–500. https://doi.org/10.1016/j.sna.2017.07.020

Kunststoffe—Messung des spezifischen elektrischen Widerstands von leitfähigen Kunststoffen. (2022). Beuth Verlag GmbH.

Kwok, S. W., Goh, K. H., Tan, Z. D., Tan, S. T., Tjiu, W. W., Soh, J. Y., Ng, Z. J., Chan, Y. Z., Hui, H. K., & Goh, K. E. (2017). Electrically conductive filament for 3D-printed circuits and sensors. *Applied Materials Today*, 9, 167–175. https://doi.org/10.1016/j.apmt.2017.07.001

Masarra, N.-A., Batistella, M., Quantin, J.-C., Regazzi, A., Pucci, M. F., El Hage, R., & Lopez-Cuesta, J.-M. (2022). Fabrication of PLA/PCL/Graphene Nanoplatelet (GNP) electrically conductive circuit using the fused filament fabrication (FFF) 3D printing technique. *Materials*, 15(3), 762. https://doi.org/10.3390/ma15030762

Nassar, H., & Dahiya, R. (2021). Fused Deposition Modeling-Based 3D-Printed Electrical Interconnects and Circuits. *Advanced Intelligent Systems*, 3. https://doi.org/10.1002/aisy.202100102

Nowka, M., Hilbig, K., Schulze, L., Heller, T., Goutier, M., & Vietor, T. (2024). Influence of Manufacturing Process on the Conductivity of Material Extrusion Components: A Comparison between Filament- and Granule-Based Processes. *Polymers*, 16(8), 1134. https://doi.org/doi.org/10.3390/polym16081134

Nowka, M., Hilbig, K., Schulze, L., Jung, E., & Vietor, T. (2023). Influence of process parameters in material extrusion on product properties using the example of the electrical resistivity of conductive polymer composites. *Polymers*, 15(22), 4452. https://doi.org/10.3390/polym15224452

Nowka, M., Ruge, K., Hilbig, K., Schulze, L., & Vietor, T. (2025). Influence of Layer Height and Nozzle Diameter on the Resistivity of Additively Manufactured Electrically Conductive Structures Made by Material Extrusion. *Rapid Prototyping Journal*. https://doi.org/10.1108/RPJ-01-2025-0014

Nowka, M., Ruge, K., Schulze, L., Hilbig, K., & Vietor, T. (2024). Characterization of the Anisotropic Electrical Properties of Additively Manufactured Structures Made from Electrically Conductive Composites by Material Extrusion. *Polymers*, 16(20). https://doi.org/10.3390/polym16202891

Paz, R., Moriche, R., Monzón, M., & García, J. (2020). Influence of manufacturing parameters and post processing on the electrical conductivity of extrusion-based 3D printed nanocomposite parts. *Polymers*, 12(4), 733. https://doi.org/10.3390/polym12040733

Rosen, D. W. (2007). Computer-Aided Design for Additive Manufacturing of Cellular Structures. *Computer-Aided Design and Applications*, 4(5), 585–594. https://doi.org/10.1080/16864360.2007.10738493

Stankevich, S., Sevcenko, J., Bulderberga, O., Dutovs, A., Erts, D., Piskunovs, M., Ivanovs, V., Ivanov, V., & Aniskevich, A. (2023). Electrical Resistivity of 3D-Printed Polymer Elements. *Polymers*, 15(14). https://doi.org/10.3390/polym15142988

Tan, J. C., & Low, H. Y. (2018). Embedded electrical tracks in 3D printed objects by fused filament fabrication of highly conductive composites. *Additive Manufacturing*, 23, 294–302. https://doi.org/10.1016/j.addma.2018.06.009

Truman, L., Whitwam, E., Nelson-Cheeseman, B. B., & Koerner, L. J. (2020). Conductive 3D printing: Resistivity dependence upon infill pattern and application to EMI shielding. *Journal of Materials Science: Materials in Electronics*, 31(17), 14108–14117. https://doi.org/10.1007/s10854-020-03965-9

https://doi.org/10.1017/pds.2026.10561 Published online by Cambridge University Press

Watschke, H., Hilbig, K., & Vietor, T. (2019). Design and characterization of electrically conductive structures additively manufactured by material extrusion. *Applied Sciences*, 9(4), 779. https://doi.org/10.3390/app9040779

Zhang, J., Yang, B., Fu, F., You, F., Dong, X., & Dai, M. (2017). Resistivity and its anisotropy characterization of 3D-printed acrylonitrile butadiene styrene copolymer (abs)/carbon black (CB) composites. *Applied Sciences*, 7(1), 20. https://doi.org/10.3390/app7010020

https://doi.org/10.1017/pds.2026.10561 Published online by Cambridge University Press